Plasma Pressure Response to Non-Inductive Current Drive in Axisymmetric Viscoresistive MHD Steady-states

Anna Krupka, Marie-Christine Firpo

Plasma Pressure Response to Non-Inductive Current Drive in Axisymmetric Viscoresistive MHD Steady-states

Anna Krupka and Marie-Christine Firpo
Laboratoire de Physique des Plasmas (LPP), CNRS, Sorbonne Université,
Ecole polytechnique, Institut Polytechnique de Paris, 91120 Palaiseau, France
(*marie-christine.firpo@lpp.polytechnique.fr)
(*anna.krupka@lpp.polytechnique.fr)
(Dated: December 12, 2024)

We investigate self-consistent, steady-state axisymmetric solutions of incompressible tokamak plasma using a visco-resistive magnetohydrodynamic model. A key contribution of this work is the formulation of Poisson's equation that governs the pressure profile. Our analysis reveals that the current modeling fails to produce realistic pressure levels. To overcome this limitation, we introduce additional non-inductive current drives, akin to those generated by neutral beam injection or radio frequency heating, modeled as modifications to the toroidal current. Numerical simulations validate our enhanced model, showing significant improvements in pressure profile characteristics. In the cases examined, the effect of these current drives on the velocity profiles is moderate, except when the non-inductive current drives induce reversals in the total toroidal current density, leading to non-nested flux surfaces with internal separatrices.

Keywords: magnetic confinement fusion; MHD; non-inductive current drive; equilibrium reconstruction

I. INTRODUCTION

Tokamaks, ideally designed with axisymmetry, are devices aimed at achieving controlled thermonuclear fusion through the magnetic confinement of plasma. A thorough understanding of tokamak plasma physics within this axisymmetric framework is crucial, as it serves as the foundation from which three-dimensional perturbations inevitably arise. To address this, we employ a steady-state, self-consistent, axisymmetric (2D) model utilizing visco-resistive magnetohydrodynamics (MHD). While more realistic models have been developed —those that (gyro-)kinetically describe each plasma species, coupled with Maxwell's equations and incorporating the external driving forces present in tokamak devices—these are known to be computationally intensive and complex. Furthermore, implementing boundary conditions in such kinetic models presents significant challenges. Therefore, a self-consistent MHD approach offers a reasonable initial step in our investigation. Moreover, the adoption of a time-independent, steady-state model is motivated by its inherent desirability for a functional fusion reactor.

In the present study, we consider then a steady-state visco-resistive MHD model compatible with tokamak operation. A key challenge in developing a minimal yet realistic model for tokamak plasmas lies in accurately representing the physical drives at work within the device. A first natural drive is the curl-free magnetic field created by the external coils. A second drive must be implemented to induce the winding of the magnetic field lines around the magnetic axis by creating a poloidal component of the magnetic field. The stationary states of the plasma under the constraint of axisymmetry can then be determined by solving the self-consistent system formed by the steady-state Navier-Stokes equation for the plasma and the steady-state Maxwell equations, including the external drives. This system can be solved, for example, by the finite element method, once the plasma domain Ω and the boundary conditions for the fields have been specified. Previous studies [1–3] have relied on models where the dependence of the visco-resistive system on these two external drives can be reformulated as a dependence on a single control parameter [4] that amounts to the ratio of the electric current induced by Ohm's law in the plasma for a given toroidal loop voltage over that needed for generating the external toroidal magnetic field. A second relevant control parameter relative to the visco-resistive framework is the Hartmann number defined as $H = (\eta\nu)^{-1/2}$, where η and ν are respectively the dimensionless plasma resistivity and viscosity.

In this setting, the plasma pressure field has been largely ignored as the pressure can be eliminated from this resolution by considering the curl of the steady-state Navier-Stokes equation. This is the manifestation of the fact, which is well-known in the study of the Navier-Stokes equation applied to neutral fluids, that pressure is not an actuator but a passive variable. In the present study, we focus on the evaluation of the pressure field, a point that has been overlooked in this approach so far. The present derivation of the pressure field will be self-consistent. This is a departure from the typical treatment of pressure in tokamak plasmas. Conventional approaches, such as real-time equilibrium reconstruction codes using the Grad-Shafranov equation, or its extended versions incorporating some plasma flows that is also known as the Grad–Shafranov–Bernoulli system of equations [5–9], treat the scalar pressure field as a free function. This function, along with the diamagnetic function (and possibly functions associated to plasma flows), is optimized to minimize the χ^2 from the measured data. In other typical models for tokamak plasmas, the pressure may be evaluated using an equation of state.

In Section II, we introduce and discuss the limitations of the aforementioned steady-state axisymmetric model for describing tokamak plasmas within a visco-resistive MHD framework having as time-independent external drives a curl-free toroidal magnetic field and a curl-free toroidal electric field (loop voltage) [1–4] . Specifically, it is predicted that this

system yields a zero pressure gradient in the ideal and motionless limit. This points to the necessity of incorporating an additional non-inductive current drive [10, 11] in a steady-state machine to effectively control and increase the pressure. This is addressed in Section II D where we implement some current drive to model the heating methods used in real tokamaks [12, 13] verified through pressure profiles in Section III. Numerical simulations with toroidal current drives are presented in Section IV, utilizing the finite element method through the open-source platform FreeFem++ for solving partial differential equations [14]. A concluding Section V summarizes the study's findings.

II. THE NECESSITY OF NON-INDUCTIVE CURRENT DRIVE: A THEORETICAL APPROACH

A. Axisymmetric steady-state visco-resistive MHD equations: Self-consistent system of equations

The framework employed in this study is magnetohydrodynamics. In more precise terms, building on the research initiated by Montgomery and his collaborators [15], we assume that the axisymmetric steady-states of the plasma are governed by the incompressible visco-resistive MHD. This is consistent with the customary reconstruction of 2D equilibria using the Grad-Shafranov equation, except that we do not assume the velocity field to be zero, and we have a self-consistent model as we do not have free functions. Then, to describe a tokamak plasma, an essential aspect is to model the external drives involved in the system. One inherent drive in this magnetic confinement fusion device is the external magnetic field. Additionally, the need to wind the magnetic field lines and create a macroscopic poloidal component of the magnetic field requires a second forcing mechanism. Following previous references [1–4], we assume that the poloidal magnetic field component is generated by a toroidal electric field, which drives a toroidal current density.

Denoting by B_0 the value of the external magnetic field on the magnetic axis, by μ_0 the vacuum permeability and by ρ_{m0} the plasma mass density assumed to be constant, the Alfvén velocity is $v_{A0} = B_0/(\mu_0\rho_{m0})^{1/2}$. In the remainder of this article, we shall work with dimensionless variables. Specifically, velocities are normalized with respect to the Alfvén speed, v_{A0}, as is the field $\boldsymbol{B}/(\mu_0\rho_{m0})^{1/2}$. Moreover, the space variables are also dimensionless. From the set of cylindrical polar coordinates (R,φ,Z) and denoting by R_0 the tokamak major radius, we define $r = R/R_0$ and $z = Z/R_0$. The computation of visco-resistive axisymmetric steady states involves then solving the steady-state incompressible Navier–Stokes equation (1)-(2) along with the solenoidal condition (3), Faraday's law (4), Ampère law (5) and Ohm's law (6) on a tokamak poloidal plasma cross-section Ω. The equations are

$$(\boldsymbol{v}\cdot\nabla)\boldsymbol{v} = \boldsymbol{J}\times\boldsymbol{B} - \nabla p + \nu\nabla^2\boldsymbol{v}, \tag{1}$$
$$\nabla\cdot\boldsymbol{v} = 0, \tag{2}$$
$$\nabla\cdot\boldsymbol{B} = 0, \tag{3}$$
$$\nabla\times\boldsymbol{E} = 0, \tag{4}$$
$$\nabla\times\boldsymbol{B} = \boldsymbol{J}, \tag{5}$$
$$\boldsymbol{E} + \boldsymbol{v}\times\boldsymbol{B} = \eta\boldsymbol{J}. \tag{6}$$

With respect to the drives, both the externally applied (vacuum) toroidal magnetic field and the steady-state toroidal electric field required to drive the toroidal current are curl-free. We have

$$\boldsymbol{B}_{\text{ext}} = \frac{1}{r}\boldsymbol{i}_\varphi, \tag{7}$$
$$\boldsymbol{E}_{\text{ext}} = \frac{E_0}{r}\boldsymbol{i}_\varphi, \tag{8}$$

with $\boldsymbol{i}_\varphi$ a unit vector in the toroidal (azimuthal) direction. The magnetic and electric fields in Eqs. (1)-(6) are the sum of these external contributions and of the self-consistent plasma fields. This system of equations needs to be solved on the plasma cross-section Ω with suitable boundary conditions. From a computational perspective, we solve the system of partial differential equations (PDE) that we are now presenting.

B. Scalar PDE formulation

One can eliminate the unknown pressure term by taking the curl of Eq. (1). This signifies that the pressure is a passive variable and not an actuator. Moreover, the velocity $\boldsymbol{v}$, vorticity $\boldsymbol{\omega}\equiv\nabla\times\boldsymbol{v}$, magnetic $\boldsymbol{B}$ and current density $\boldsymbol{J}$ vector fields are divergence-free, they admit then the following representations

$$\boldsymbol{v} = \frac{1}{r}\nabla\chi\times\boldsymbol{i}_\varphi + v_\varphi\boldsymbol{i}_\varphi, \tag{9}$$
$$\boldsymbol{\omega} = \frac{1}{r}\nabla\left(rv_\varphi\right)\times\boldsymbol{i}_\varphi - \frac{1}{r}\left(\triangle^*\chi\right)\boldsymbol{i}_\varphi, \tag{10}$$
$$\boldsymbol{B} = \frac{1}{r}\nabla\psi\times\boldsymbol{i}_\varphi + B_\varphi\boldsymbol{i}_\varphi, \tag{11}$$
$$\boldsymbol{J} = \frac{1}{r}\nabla\left(rB_\varphi\right)\times\boldsymbol{i}_\varphi - \frac{1}{r}\left(\triangle^*\psi\right)\boldsymbol{i}_\varphi, \tag{12}$$

where χ is the velocity stream function, ψ is the magnetic flux function, B_φ is the toroidal component of the magnetic field vector and v_φ is the toroidal component of the velocity field vector. The above system of equations (1)-(6) with the external drives (7)-(8) can be expressed [1, 2, 4, 15, 16] as the

following set of five scalar elliptic PDE

$$\triangle^* \chi = -r\omega_\varphi, \tag{13}$$

$$\nu \triangle^* (r\omega_\varphi) = \frac{1}{r^2}\frac{\partial}{\partial z}((rB_\varphi)^2 - (rv_\varphi)^2) + \frac{1}{r}\{rj_\varphi, \psi\} \tag{14}$$

$$+ \frac{1}{r}\{\chi, r\omega_\varphi\} + \frac{2\omega_\varphi}{r}\frac{\partial \chi}{\partial z} - \frac{2j_\varphi}{r}\frac{\partial \psi}{\partial z}, \tag{15}$$

$$\eta \triangle^* (rB_\varphi) = \frac{1}{r}\{\chi, rB_\varphi\} + \frac{1}{r}\{rv_\varphi, \psi\} + \tag{16}$$

$$+ \frac{2rB_\varphi}{r^2}\frac{\partial \chi}{\partial z} - \frac{2v_\varphi}{r}\frac{\partial \psi}{\partial z}, \tag{17}$$

$$\nu \triangle^* (rv_\varphi) = \frac{1}{r}\{\chi, rv_\varphi\} + \frac{1}{r}\{rB_\varphi, \psi\}, \tag{18}$$

$$\triangle^* \psi = -rj_\varphi, \tag{19}$$

with the toroidal projection of Ohm's law giving the constraint

$$\eta r j_\varphi = E_0 + \frac{1}{r}\{\psi, \chi\}. \tag{20}$$

Here, the Poisson bracket $\{u, v\}$ for any spatial functions u and v is defined as

$$\{u, v\} \equiv \frac{\partial u}{\partial r}\frac{\partial v}{\partial z} - \frac{\partial v}{\partial r}\frac{\partial u}{\partial z}, \tag{21}$$

and the operator $\triangle^*$ is defined by

$$\triangle^* A \equiv \frac{\partial^2 A}{\partial r^2} - \frac{1}{r}\frac{\partial A}{\partial r} + \frac{\partial^2 A}{\partial z^2}. \tag{22}$$

A relevant dimensionless control parameter has been identified [4, 17, 18] as the Hartmann number, $H = (\eta\nu)^{-1/2}$. In fusion-relevant conditions, this is expected to be a large parameter, ranging from 10^6 to 10^8. Simulations for realistic parameter values already exist for this system under various boundary conditions, typically using the JET geometry. The elliptic system (13)–(19) requires five boundary conditions. The four conditions associated with the divergence-free properties of the magnetic field ($\boldsymbol{B}$), current density ($\boldsymbol{J}$), velocity ($\boldsymbol{V}$), and vorticity ($\boldsymbol{\omega}$) vector fields are determined by ensuring the continuity of their normal components across the plasma boundary. The following boundary conditions are selected in the numerical simulations: $\chi = \psi = 0$ and $B_\varphi = 1/r$ on $\partial\Omega$. We enforce Neumann boundary conditions on both the toroidal velocity v_φ and toroidal vorticity ω_φ through $\partial_n v_\varphi = \partial_n \omega_\varphi = 0$ on $\partial\Omega$. We used the open-source PDE solver FreeFem++, employing the finite element method [14] to solve the above steady-state axisymmetric system of equations in a weak form on the plasma cross-section domain Ω with the specified boundary conditions. For our calculations, we set a tolerance parameter $\varepsilon = 10^{-10}$, allowing the Newton-Raphson scheme to converge in typically 4–5 iterations.

C. Examination of the pressure field

Let us now examine the pressure profile in the visco-resistive model (1)-(6) with the external drives (7)-(8). Let us assume for now that the steady-state plasma speed is negligible. Then, in the ideal limit, $\eta \to 0$ and $\nu \to 0$, the steady-state Navier-Stokes equation (1) takes the form

$$\nabla p = \boldsymbol{J} \times \boldsymbol{B}. \tag{23}$$

Restricting to axisymmetric solutions, the projection of this equation on r and z gives, respectively,

$$\frac{\partial p}{\partial r} = r^{-1}\left(-B_\varphi \frac{\partial (rB_\varphi)}{\partial r} + j_\varphi \frac{\partial \psi}{\partial r}\right), \tag{24}$$

$$\frac{\partial p}{\partial z} = r^{-1}\left(-B_\varphi \frac{\partial (rB_\varphi)}{\partial z} + j_\varphi \frac{\partial \psi}{\partial z}\right). \tag{25}$$

In the toroidal direction, we get

$$0 = r^{-2}\{\psi, rB_\varphi\} \tag{26}$$

which amounts to the well-known property of Grad-Shafranov's theory that the diamagnetic function, rB_φ, is a function of the magnetic flux ψ only. Moreover, writing that $\boldsymbol{J} \times \boldsymbol{B}$ is curl-free, which follows from the force balance equation (23) and projecting this on the toroidal direction yields

$$-2rB_\varphi \frac{\partial B_\varphi}{\partial z} + \{\psi, rj_\varphi\} + 2rj_\varphi \frac{\partial \psi}{\partial z} = 0. \tag{27}$$

Then, combining Eqs. (25) and (27), the pressure gradient along the z-axis with a zero-flow hypothesis is given by

$$\frac{\partial p}{\partial z} = \frac{1}{2r}\{rj_\varphi, \psi\}. \tag{28}$$

Yet, assuming no plasma flow, the toroidal projection of Ohm's law in Eq. (20) states that rj_φ is a constant, with $rj_\varphi = E_0/\eta$. Eq. (28) indicates then that the pressure field does not depend on z. However, from the set of equations (24)–(25)–(26), we can deduce that the pressure is a function of the magnetic flux ψ such that $\{p, \psi\} = 0$. Thus, we have $\partial_z p = p'(\psi)\partial_z \psi = 0$. This implies that the pressure profile is constant. This aligns with the results obtained by [19], which indicate that in equilibrium configurations, the current density must be proportional to $1/r$ when the pressure gradient is zero.

D. Implications and implementation of non-inductive current drives

Section II C demonstrates that the sole inclusion of Ohm's law to close the system imposes significant limitations on the model. Specifically, the effective pressure in the model arises only because the toroidal geometry and viscous dissipation prevent the steady-state velocity field from being identically zero. This allows the pressure profile to remain non-zero, as rj_φ is not exactly constant. However, the model lacks a robust mechanism to provide sufficient heating to achieve fusion conditions. Therefore, incorporating alternative heating methods is essential for attaining higher pressure. We will also see

that this tends to induce higher plasma rotation velocities in specific drive configurations.

In our previous analysis, we focused on the behaviour of the system for a specific ratio of E_0/η, which was the only explicit drive in the dimensionless system of equations [4]. Now, we aim to introduce an additional drive which will manifest as an extra term in the toroidal component of Ohm's law in Eq. (6) with

$$\frac{E_0}{r}+(\boldsymbol{v}\times\boldsymbol{B})\cdot\boldsymbol{i}_\varphi+j_D=\eta\boldsymbol{J}\cdot\boldsymbol{i}_\varphi, \tag{29}$$

where j_D represents a current drive. Eq. (20) now becomes

$$\eta r j_\varphi = E_0+\frac{1}{r}\{\psi,\chi\}+j_D r. \tag{30}$$

Our goal is to investigate the influence of the non-inductive current drive j_D within our system. We will begin by evaluating its effect on the pressure profile. For this purpose, it is necessary to determine the pressure field, which we will now establish.

III. DERIVATION OF POISSON'S EQUATION FOR THE PRESSURE FIELD

Let us go back to the steady-state Navier-Stokes equation (1) and rewrite it as

$$\boldsymbol{\omega}\times\boldsymbol{v}=\boldsymbol{J}\times\boldsymbol{B}-\nabla p^*+\nu\nabla^2\boldsymbol{v} \tag{31}$$

with

$$p^*=p+\frac{v^2}{2}. \tag{32}$$

Previously, we eliminated the pressure term by taking the curl and considering the toroidal part of the force balance equation. Now, to obtain the pressure of the system, we take the divergence of Eq. (31)

$$\nabla\cdot\nabla p^*=\nabla\cdot\left[-\boldsymbol{\omega}\times\boldsymbol{v}+\boldsymbol{J}\times\boldsymbol{B}+\nu\nabla^2\boldsymbol{v}\right]. \tag{33}$$

This takes the form of Poisson's equation for the pressure p^* as the left-hand side yields the Laplacian of the pressure, $\triangle p^*$. Taking the divergence of the first term on the right-hand side gives

$$-\nabla\cdot(\boldsymbol{\omega}\times\boldsymbol{v})=\boldsymbol{v}\cdot\nabla^2\boldsymbol{v}+\boldsymbol{\omega}^2. \tag{34}$$

We can treat the $\boldsymbol{J}\times\boldsymbol{B}$ term similarly

$$\nabla\cdot(\boldsymbol{J}\times\boldsymbol{B})=-\boldsymbol{B}\cdot\nabla^2\boldsymbol{B}-\boldsymbol{J}^2. \tag{35}$$

Finally, the term $\nabla\cdot(\nu\nabla^2\boldsymbol{v})$ equals zero due to the incompressibility condition $\nabla\cdot\boldsymbol{v}=0$. Therefore, the complete Poisson's equation for the pressure is

$$\triangle p^*=\boldsymbol{v}\cdot\nabla^2\boldsymbol{v}+\boldsymbol{\omega}^2-\boldsymbol{B}\cdot\nabla^2\boldsymbol{B}-\boldsymbol{J}^2 \tag{36}$$

where $\triangle$ is defined as

$$\triangle A\equiv\frac{\partial^2 A}{\partial r^2}+\frac{1}{r}\frac{\partial A}{\partial r}+\frac{\partial^2 A}{\partial z^2}. \tag{37}$$

Next, we will express the Poisson's equation (36) in terms of the functions $\chi,\ldots,j_\varphi$ defined over the domain $(r,z)\in\Omega$. To do this, we will analyze each term separately. By utilizing the expression for the vorticity (10), the second term can be rewritten as

$$\boldsymbol{\omega}^2=-\frac{\omega_\varphi}{r}\triangle^*\chi+\left(\frac{1}{r}\frac{\partial(rv_\varphi)}{\partial r}\right)^2+\left(\frac{\partial v_\varphi}{\partial z}\right)^2. \tag{38}$$

Similarly, for the square of the current density vector (12), we get

$$\boldsymbol{J}^2=-\frac{j_\varphi}{r}\triangle^*\psi+\left(\frac{1}{r}\frac{\partial(rB_\varphi)}{\partial r}\right)^2+\left(\frac{\partial B_\varphi}{\partial z}\right)^2. \tag{39}$$

Finally, let us examine the term $\boldsymbol{B}\cdot\nabla^2\boldsymbol{B}$. We can use the identity $\boldsymbol{B}\cdot\nabla^2\boldsymbol{B}=-\boldsymbol{B}\cdot(\nabla\times\boldsymbol{J})$ with

$$\boldsymbol{B}\cdot(\nabla\times\boldsymbol{J})=-\frac{B_\varphi}{r}\triangle^*(rB_\varphi)+\frac{1}{r^2}\frac{\partial\psi}{\partial r}\frac{\partial(rj_\varphi)}{\partial r}+\frac{1}{r}\frac{\partial\psi}{\partial z}\frac{\partial j_\varphi}{\partial z}. \tag{40}$$

Similarly, we have

$$\boldsymbol{v}\cdot(\nabla\times\boldsymbol{\omega})=-\frac{v_\varphi}{r}\triangle^*(rv_\varphi)+\frac{1}{r^2}\frac{\partial(r\omega_\varphi)}{\partial r}\frac{\partial\chi}{\partial r}+\frac{1}{r}\frac{\partial\omega_\varphi}{\partial z}\frac{\partial\chi}{\partial z}. \tag{41}$$

Incorporating all of these contributions into the right-hand side of Poisson's equation yields

$$\begin{aligned}\triangle p^*=&\frac{v_\varphi}{r}\triangle^*(rv_\varphi)-\frac{1}{r^2}\frac{\partial(r\omega_\varphi)}{\partial r}\frac{\partial\chi}{\partial r}-\frac{1}{r}\frac{\partial\omega_\varphi}{\partial z}\frac{\partial\chi}{\partial z}\\&-\frac{\omega_\varphi}{r}\triangle^*\chi+\left(\frac{1}{r}\frac{\partial(rv_\varphi)}{\partial r}\right)^2+\left(\frac{\partial v_\varphi}{\partial z}\right)^2\\&-\frac{B_\varphi}{r}\triangle^*(rB_\varphi)+\frac{1}{r^2}\frac{\partial\psi}{\partial r}\frac{\partial(rj_\varphi)}{\partial r}+\frac{1}{r}\frac{\partial\psi}{\partial z}\frac{\partial j_\varphi}{\partial z}\\&+\frac{j_\varphi}{r}\triangle^*\psi-\left(\frac{1}{r}\frac{\partial(rB_\varphi)}{\partial r}\right)^2-\left(\frac{\partial B_\varphi}{\partial z}\right)^2.\end{aligned} \tag{42}$$

This elliptic differential equation needs to be solved with a boundary condition and allow the pressure profiles for the different drives to be computed. To the best of our knowledge, the derivation of Eq. (42) within the visco-resistive system is novel.

IV. NUMERICAL RESULTS

A. Pressure field behavior without and with non-inductive current drives

Let us now solve Poisson's equation for pressure, assuming a zero pressure condition at the boundary $\partial\Omega$. It is important to note that, in the absence of an additional toroidal

current drive and assuming no plasma flow, we previously inferred a zero pressure gradient, resulting in a constant zero pressure in the limits $\eta \to 0$ and $\nu \to 0$, as discussed in Section II C. To return to dimensional pressure and compare the results with those obtained from the JET tokamak, we recall that p^* is the dimensionless total pressure [4], normalized as $p^* = \hat{p}^*/v_{A0}^2\rho_m$, where $\hat{p}^*$ is dimensional pressure. By using parameters from a specific JET deuterium-tritium shot [20], we obtain $\rho_m = 2.09 \cdot 10^{-7}\,\mathrm{kg/m^3}$ and the Alfvén velocity $v_{A0} = 5.46 \cdot 10^6\,\mathrm{m/s}$. To verify the pressure distribution in the absence of the drive with plasma flow, let us examine Fig. 1. The pressure profile is presented in Pascal units (Pa). The order of magnitude of the pressure field in the absence of the current drive turns out to be unrealistically small, as predicted in Section II C.

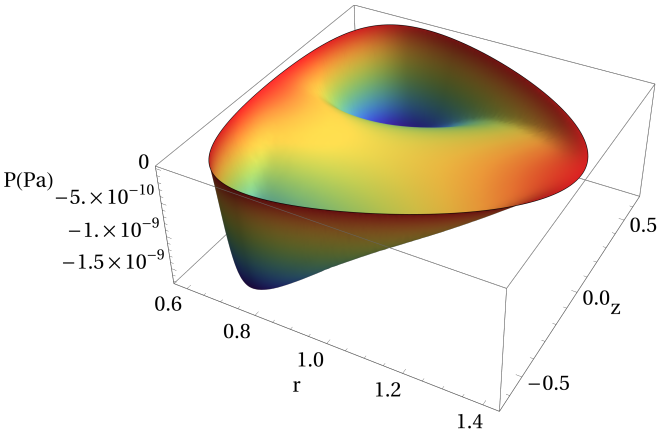

FIG. 1. Pressure field in Pascal units computed without the application of the drive ($j_D = 0$) for a Hartmann number of $H = 10^5$.

To explore the effects of a non-inductive current drive, we considered a family of drives, j_D, which are solutions to the Poisson's equation $\nabla^2 j_D = -A$, with the boundary condition $j_D = B$ on $\partial\Omega$. Here, A denotes the magnitude of the drive, while B represents the current distribution offset. This approach provides an initial method for simulating current distributions akin to those generated by heating mechanisms in tokamaks, effectively "adding a bump" to the current profile. Let us now choose a drive that produces realistic pressure profiles. To do so, we select j_D with $A = 100$ and $B = 0$. Fig. 2 compares the toroidal current density fields, calculated at Hartmann number $H = 10$, using Eqs. (13)–(19) for $j_D = 0$ (the reference case) and for j_D with $A = 100$ and $B = 0$. In the original system [1–4] ($j_D = 0$), the model fails to produce realistic toroidal current density profiles despite yielding a realistic total current. This is because a ratio of E_0/η of approximately one corresponds to a realistic total current for the JET deuterium-tritium shot [20].

Let us now examine how the application of the drive affects the pressure profiles. Fig. 3 shows the computed pressure, $p = p^* - v^2/2$, with the application of the drive j_D using $A = 100$ and $B = 0$ for $H = 10^5$. The drive not only prevents unrealistically low pressure levels but also achieves pressure values comparable to those observed in the JET tokamak [20].

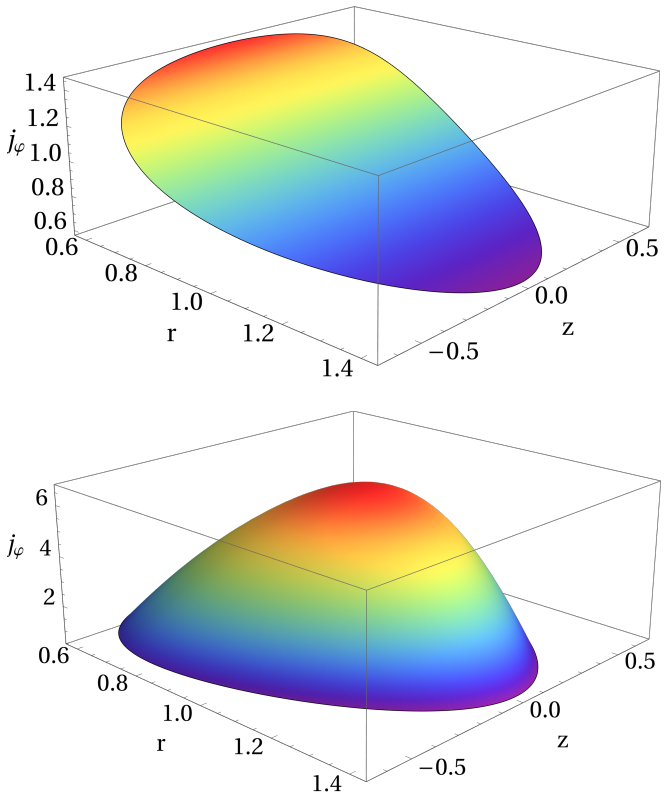

FIG. 2. Toroidal current field without the drive ($j_D = 0$) (at the top) and with the drive j_D set to $A = 100$ and offset $B = 0$ (at the bottom) for a Hartmann number of $H = 10$ in dimensionless units.

Let us now examine how the variation of the magnitude of the drive affects the root-mean-square of the pressure as a function of the Hartmann number. Fig. 4 illustrates this relationship. It is evident that all the magnitudes A of the drive j_D chosen in this study produce a realistic pressure response.

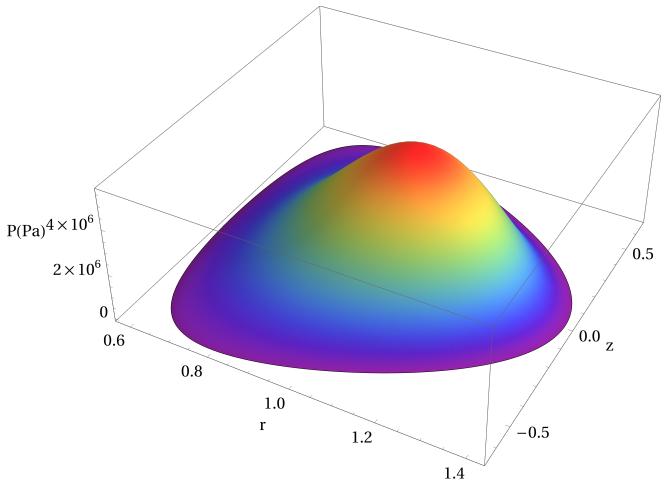

FIG. 3. Pressure field in Pascal units computed with the application of the drive j_D with $A = 100$ and $B = 0$ on the toroidal current density field. The Hartmann number is $H = 10^5$.

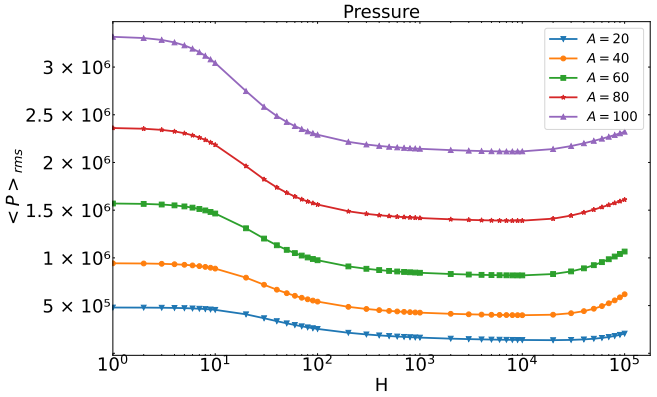

FIG. 4. Root mean square of the pressure field in pascals as a function of the Hartmann number, with the application of the drive j_D with $B = 0$ on the toroidal current field, for various values of A.

Let us note that, with the application of the drives, it is possible to achieve various configurations of magnetic flux surfaces, including non-nested magnetic field lines with several $n = 0$ islands present. Such an example is given in Fig. 5 that shows the magnetic flux surfaces and the pressure profile when the drive j_D with $A = 100$ and $B = -5$ is applied. However, we will primarily focus on drives that induce standard nested magnetic flux surfaces.

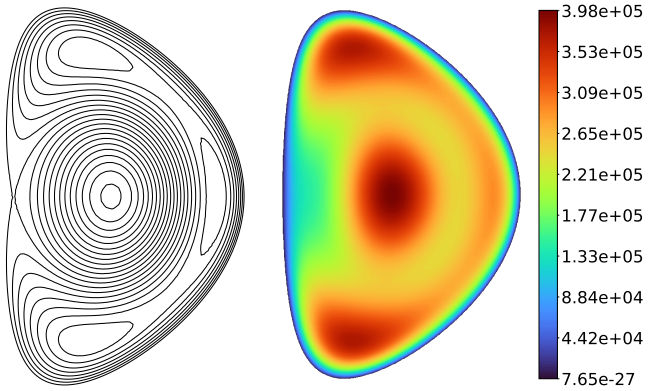

FIG. 5. Magnetic flux surfaces with internal separatrices (on the left) and pressure profiles (on the right) computed with the application of the drive j_D with $A = 100$ and $B = -5$ on the toroidal current field for $H = 10^5$.

B. Impact of the non-inductive current drive on steady-state velocity and scaling

Let us now examine the impact on the velocity distribution of the application of the current drive j_D. Fig. 6 presents the root-mean-square of the toroidal velocity field while applying the drive j_D with $B = 0$ to the toroidal current field across various values of A, as in Fig. 4. It can be observed that while varying the magnitude of the drive causes an increase in velocities in the low-H regime, the large-H, boundary layer, regime remains almost unchanged despite the application of current drives with different magnitudes. Increasing the magnitude raises the total current, but the velocities seem unaffected by this variation.

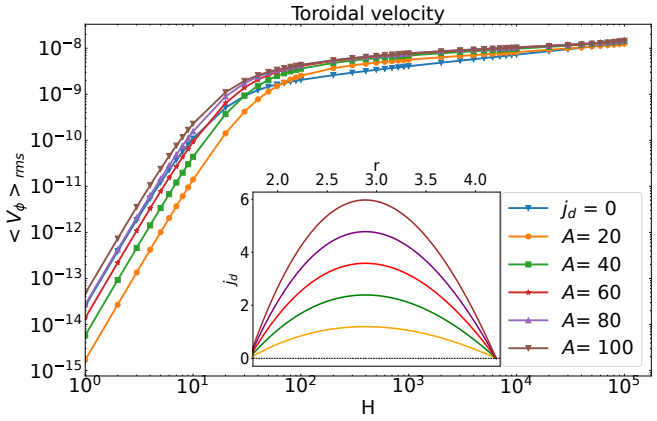

FIG. 6. Root mean square of toroidal velocity in Alfvén velocity units as a function of the Hartmann number, considering the application of the drive j_D with $B = 0$ on the toroidal current field, for the different values of A.

Next, let us examine how the velocities change with the variation of the parameter B, which represents the offset of the drive j_D. Fig. 7 presents the same information as Fig. 6, but with a fixed value of $A = 100$ while exploring different values of B. Shifting the drive results in the highest velocities at $B = -5$. It is evident that the usual large-H velocity behavior changes at certain parameters of the current drive.

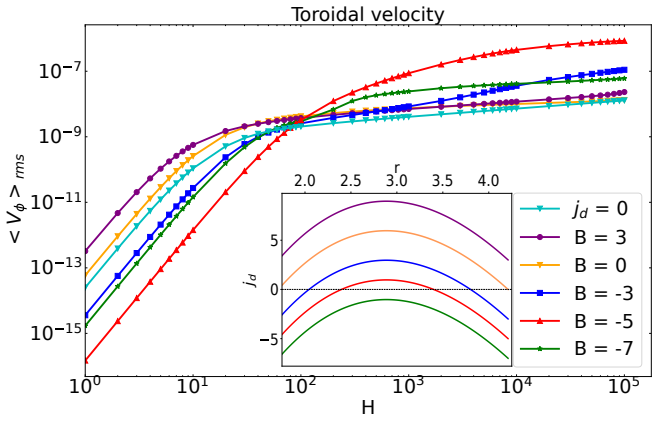

FIG. 7. Root mean square of toroidal velocity in Alfvén velocity units as a function of the Hartmann number, considering the application of the drive j_D with $A = 100$ on the toroidal current field, for various values of B.

Indeed, in the high-Hartmann number regime, two scenarios emerge: either the boundary layer forms [4], and the root-mean-square of the toroidal and poloidal velocities exhibit some scaling law with the Hartmann number, as is the case for the drive j_D with $B = 0$ and $B = 3$; or the velocities do not develop a linear behavior on a log-log scale for $B = -3$,

-5, and -7, meaning that the velocities do not scale with the Hartmann number. Let us now take a closer look at this latest phenomenology, which is novel and pertains to a situation involving non-nested magnetic flux surfaces with internal separatrices. To illustrate this, we examine the non-inductive current drive j_D with $A = 100$ and $B = -5$ for $H = 10^5$, where the magnetic flux surfaces and pressure field are depicted in Fig. 5. Fig. 8 shows on the left the associated toroidal current field.

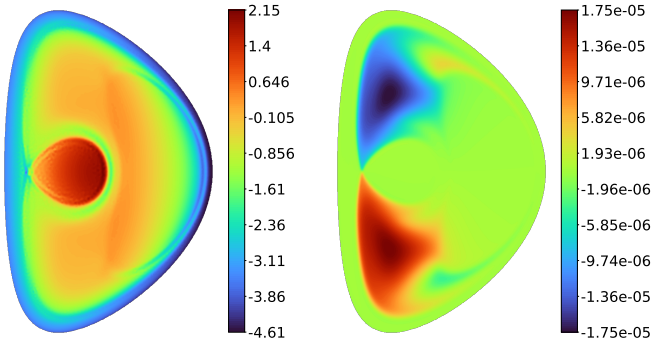

FIG. 8. Toroidal current density field (on the left) and toroidal velocity field (on the right) with the application of the drive j_D with $A = 100$, $B = -5$ for $H = 10^5$ as in Fig. 5.

The velocity distribution on the right of Fig. 8 closely resembles the toroidal current distribution, with the highest velocities occurring at the transition point between positive and negative current regions. In this case, we observe no formation of a boundary layer, which is advantageous from a numerical perspective. The absence of a boundary layer contributes to increased stability in the code and yields more robust results. There is significant potential to achieve much higher velocities with these drives; however, accurately predicting which current drive would be optimal for maximizing velocities remains a challenge and necessitates further investigation.

V. CONCLUSION AND PERSPECTIVES

We have examined the axisymmetric steady states of tokamak plasmas using an incompressible visco-resistive MHD model. In addition to the intrinsic limitations of a magnetohydrodynamic rather than a kinetic approach, a crucial point in the search for a relevant minimal model lies in modelling and implementing the drives at work in a tokamak device. In some previous modelings [1–4], apart from the external, given, vacuum magnetic field, the ratio E_0/η was the only drive in the system. A significant advancement of the present study is the formulation of Poisson's equation governing the pressure within a self-consistent visco-resistive MHD framework. This approach differs notably from the Grad-Shafranov method used in equilibrium reconstruction, where pressure is treated as a free function. The numerical solution of this Poisson equation for pressure using the finite element method has demonstrated the necessity of implementing additional drives to avoid unrealistic pressure profiles with zero gradients in the ideal and no-flow limit. We have shown that this can be achieved through non-inductive-like current drives, resulting in realistic pressure profiles.

We examined a family of functions to model the non-inductive current drives of tokamaks, but further research is needed to optimize the distribution of non-inductive currents and make them more realistic. Another goal is to maximize their effectiveness in enhancing plasma speed and achieving fusion-relevant pressure profiles. Notably, certain configurations of our test current drives led to the formation of internal separatrices and non-nested magnetic flux surfaces, indicating the potential for more complex equilibrium structures under specific plasma conditions.

Finally, the resulting toroidal current profiles were found to depend on the Hartmann number. This suggests that future implementations of these drives could involve fixed toroidal current density profiles that are independent of other system parameters. This topic will be explored further in subsequent work.

ACKNOWLEDGMENTS

This work has been carried out within the framework of the EUROfusion Consortium and has received funding from the Euratom Research and Training Programme 2014-2018 under grant agreement No 633053. The views and opinions expressed herein do not necessarily reflect those of the European Commission.

[1] L. P. Kamp and D. C. Montgomery. Toroidal flows in resistive magnetohydrodynamic steady states. *Physics of Plasmas*, 10:157–167, 2003.

[2] Leon P. Kamp and David C. Montgomery. Toroidal steady states in visco-resistive magnetohydrodynamics. *Journal of Plasma Physics*, 70(2):113–142, April 2004.

[3] H. Oueslati, T. Bonnet, N. Minesi, M.-C. Firpo, and A. Salhi. Numerical derivation of steady flows in visco-resistive magnetohydrodynamics for JET and ITER-like geometries with no symmetry breaking. *AIP Conference Proceedings*, 2179:020009, 2019.

[4] A. Krupka and M.-C. Firpo. Scaling laws of the plasma velocity in visco-resistive magnetohydrodynamic systems. *Fundamental Plasma Physics*, 10:100044, 2024.

[5] L. Guazzotto, R. Betti, J. Manickam, and S. Kaye. Numerical study of tokamak equilibria with arbitrary flow. *Physics of Plasmas*, 11(2):604–614, February 2004.

[6] Haolong Li and Ping Zhu. Solving the grad–shafranov equation using spectral elements for tokamak equilibrium with toroidal rotation. *Computer Physics Communications*, 260:107264, 2021.

[7] Matteo Del Prete and Giovanni Montani. Influence of rotation on axisymmetric plasma equilibria: double-null dtt scenario. *PLASMA PHYSICS AND CONTROLLED FUSION*, 63(12), DEC 2021.

[8] D. A. Kaltsas and G. N. Throumoulopoulos. Neural network tokamak equilibria with incompressible flows. *PHYSICS OF PLASMAS*, 29(2), FEB 2022.

[9] G. F.-Torija Daza, J.M. Reynolds-Barredo, R. Sanchez, A. Loarte, and V. Tribaldos. Flipec, an ideal mhd free-boundary axisymmetric equilibrium solver in the presence of macroscopic flows. *Nuclear Fusion*, 64(8):086012, jun 2024.

[10] J. R. Ferron, L. L. Lao, T. S. Taylor, Y. B. Kim, E. J. Strait, and D. Wroblewski. Improved confinement and stability in the DIII-D tokamak obtained through modification of the current profile*. *Physics of Fluids B: Plasma Physics*, 5(7):2532–2539, July 1993.

[11] C. B. Forest, K. Kupfer, T. C. Luce, P. A. Politzer, L. L. Lao, M. R. Wade, D. G. Whyte, and D. Wròblewski. Determination of the noninductive current profile in tokamak plasmas. *Physical Review Letters*, 73(18):2444–2447, October 1994.

[12] C. Kessel, J. Manickam, G. Rewoldt, and W. M. Tang. Improved plasma performance in tokamaks with negative magnetic shear. *Physical Review Letters*, 72(8):1212–1215, February 1994.

[13] A. D. Turnbull, T. S. Taylor, Y. R. Lin-Liu, and H. St. John. High beta and enhanced confinement in a second stable core VH-mode advanced tokamak. *Physical Review Letters*, 74(5):718–721, January 1995.

[14] Frédéric Hecht. New development in FreeFem++. *Journal of Numerical Mathematics*, 20(3-4):251–265, 2012.

[15] Leon P. Kamp, David C. Montgomery, and Jason W. Bates. Toroidal flows in resistive magnetohydrodynamic steady states. *Physics of Fluids*, 10(7):1757–1766, July 1998.

[16] E. Roverc'h, H. Oueslati, and M.-C. Firpo. Steady-state flows in a visco-resistive magnetohydrodynamic model of tokamak plasmas with inhomogeneous heating. *Journal of Plasma Physics*, 87(2):905870217, April 2021.

[17] D Montgomery. Hartmann, Lundquist, and Reynolds: The role of dimensionless numbers in nonlinear magnetofluid behavior. *Plasma Physics and Controlled Fusion*, 35(SB):B105–B113, December 1993.

[18] S. Cappello and D. F. Escande. Bifurcation in Viscoresistive MHD: The Hartmann Number and the Reversed Field Pinch. *Physical Review Letters*, 85(18):3838–3841, October 2000.

[19] B J Braams. The interpretation of tokamak magnetic diagnostics. *Plasma Physics and Controlled Fusion*, 33(7):715, jul 1991.

[20] JET Team. Fusion energy production from a deuterium-tritium plasma in the jet tokamak. *Nuclear Fusion*, 32(2):187, feb 1992.